4-3-2018

Electronic and quantum transport properties of a graphene-BN dot-ring hetero-nanostructure

Max Seel
Michigan Technological University, seel@mtu.edu

Ravindra Pandey
Michigan Technological University, pandey@mtu.edu

Recommended Citation

Seel, M., & Pandey, R. (2018). Electronic and quantum transport properties of a graphene-BN dot-ring hetero-nanostructure. *Journal of Physics Communications, 2*(4), 1-9. http://dx.doi.org/10.1088/2399-6528/aab7df
Retrieved from: https://digitalcommons.mtu.edu/michigantech-p/399

Follow this and additional works at: https://digitalcommons.mtu.edu/michigantech-p

 Part of the Physics Commons

Electronic and quantum transport properties of a graphene-BN dot-ring hetero-nanostructure

Journal of Physics Communications

OPEN ACCESS

RECEIVED
1 November 2017

REVISED
9 March 2018

ACCEPTED FOR PUBLICATION
19 March 2018

PUBLISHED
3 April 2018

PAPER

Electronic and quantum transport properties of a graphene-BN dot-ring hetero-nanostructure

Max Seel and Ravindra Pandey

Department of Physics, Michigan Technological University, Houghton, MI 49931, United States of America

E-mail: seel@mtu.edu

Keywords: quantum dot, quantum ring, dot-ring nanostructure, graphene, boron nitride, quantum transport, nanoelectronics

Abstract

Quantum dots, quantum rings, and, most recently, quantum dot-ring nanostructures have been studied for their interesting potential applications in nanoelectronic applications. Here, the electronic properties of a dot-ring hetero-nanostructure consisting of a graphene ring and graphene dot with a hexagonal boron nitride (h-BN) ring serving as barrier between ring and dot are investigated using density functional theory. Analysis of the character of the wave functions near the Fermi level and of the charge distribution of this dot-ring structure and calculations of the quantum transport properties find asymmetry in the conductance resonances leading to asymmetric I–V characteristics which can be modified by applying a negative voltage potential to the central graphene dot.

1. Introduction

Ever since the experimental discovery of graphene [1] an immense body of theoretical and experimental work has accumulated [2] that explores the unusual conduction and transport properties (for a review see for example [3]) and possible applications in nanoelectronics and nanooptical devices. Electronic, magnetic, and optical properties of graphene quantum dots (QD) [4, 5], graphene nanoribbons [6, 7], and graphene quantum rings (QR) [8] have been analyzed. Topics include edge states in graphene rings [9], magnetic field effects [10], gated rings [11], triangular rings [12], geometry effects and edge effects as obtained in tight binding and Dirac models [13], to name just a few. A recent example of the unusual quantum transport properties of graphene nanostructures is a gate-voltage-tunable graphene-boron nitride (BN) resonant tunneling transistor [14]. Growth, chemical topology, and electronic properties of a lateral graphene-BN heterostructure were investigated in a first principle study [15]. The fabrication of graphene dots with well-defined shapes remains certainly a challenge though a possible experimental realization by using carbon nanotubes as masks in an edging process has been proposed [12].

Recently, a novel nanostructure that consists of a quantum dot surrounded by a quantum ring with a potential barrier between these parts was proposed and its transport properties have been investigated [16, 17]. It was shown that the wave function of this dot-ring nanostructure (DRN) can be shifted from the dot to the ring by tuning the position of the QD potential which can be realized by an appropriate gate voltage applied to the central dot part.

In this paper we now explore whether a DRN can be realized by using a graphene ring, an inner graphene dot, and a hexagonal boron nitride (h-BN) ring serving as barrier between outer graphene ring and central dot. The nanostructure for which first principle calculations are performed is shown in figure 1. After an analysis of the energy level structure of this graphene-h-BN DRN, of the charge distribution and the electrostatic potential, quantum transport properties are investigated. It is found that asymmetry in the conductance resonances leads to asymmetric I–V characteristics which can be modified by applying a negative voltage potential to the central graphene dot.

2. Method and computational details

The graphene-h-BN dot-ring hetero-nanostructure consists of an outer ring with 168 C atoms and zigzag edges, an inner dot with 96 C atoms, and a BN ring with 60 B and 60 N atoms (see figure 1) . The dangling bonds at the

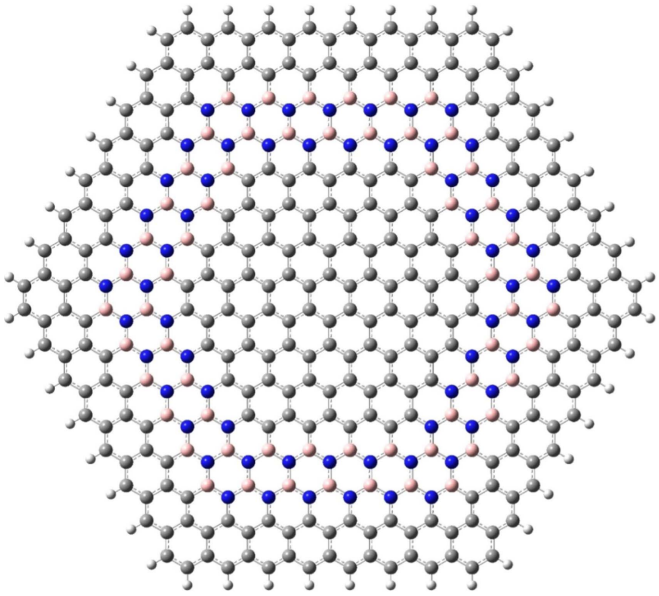

Figure 1. The graphene-BN dot-ring hetero-nanostructure with a diameter of 37 Å: an outer ring with 168 C atoms (grey), an inner dot with 96 C atoms, a BN ring with 60 B (pink) and 60 N (blue) atoms, and 48 H atoms (white) to passivate the dangling bonds of the carbon edge atoms.

edges are passivated with 48 H atoms to ensure that each boundary carbon atom has the correct number of neighbors simulating sp^2 bonding character. The DRN consists of a total of 432 atoms and has a diameter of 37 Å. Calculations were also performed for the individual parts of the system, i.e., for the C188H84 ring, the B60N60H60 ring, and for the C96H24 inner dot (the number of H atoms is determined by the number of edge atoms).

All calculations were performed with GAUSSIAN09 [18] using density functional theory (DFT) with Becke's 3-parameter hybrid functional B3LYP [19] with non-local correlation provided by the Lee, Yang, and Parr (LYP) expression [20]. Since in this exploratory study we are only interested in basic trends and not absolute quantitative numbers, the experimental values of the bond lengths for graphene and BN monolayer were used. No geometry optimization was performed. The 6-31 basis set instead of the more commonly employed 6-31(d,p) basis set was used (the B3LYP 6-31(d,p) level of theory has become a standard for a reasonable balance between accuracy and computer time for larger systems when compared to available experimental data). A direct comparison of 6-31 and 6-31(d,p) basis sets results for C96H24 (912 versus 1560 basis functions) shows that the gap between the highest occupied (HOMO) and lowest unoccupied molecular orbital (LUMO) of the graphene dot changes only from 1.95 eV to 1.93 eV with no qualitative differences in the the nature of the wave functions or charge density population. Using the 6-31 basis set the DRN system with 432 atoms has 3552 basis functions. A more detailed discussion of B3LYP results for graphene quantum dots, comparison to available experimental data, and insights gained from electronic structure calculations can be found in [21].

To demonstrate possible applications of the proposed dot-ring hetero-structure in nanoelectronic devices we compute its quantum transport properties in the tight binding approximation using the open software package Kwant [22]. The program package Kwant provides an easy way for exploratory calculations to compute the conductance using the Landauer-Büttiker formalism [23, 24]. For the tight binding Hamiltonian in the first neighbor approximation

$$H = \sum u_i |i\rangle \langle i| + \sum t_{ij} |i\rangle \langle j| \tag{1}$$

where i and j label nearest neighbor sites on a hexagonal lattice, we chose $u_C = 0$ eV, $u_N = -1.0$ eV, and $u_B = 3.6$ eV for the onsite parameters [25, 26] and the same hopping parameter $t_{ij} = t = -2.7$ eV for all first neighbor interactions. It is not to be expected that taking into account more neighbors interactions or more fine-tuned hopping parameters (e.g. $t_{BN} = -2.5$ eV, $t_{CN} = -2.3$ eV, $t_{CB} = -2.1$ eV) will change the qualitative features of the quantum transport results. Earlier tight binding results [26] for quantum transport in graphene–boron nitride lateral heterostructures corroborate the importance of the sign difference in the on-site parameters for N and B in the lattice and the robustness of the results with regard to small changes in the hopping parameters.

Kwant also allows easily to take into account the effect of a magnetic field by using Peierls substitution [27, 28] to include a vector potential $\hat{\mathbf{A}} = (-B.y, 0, 0)$ in the hopping parameter (Landau gauge for a constant

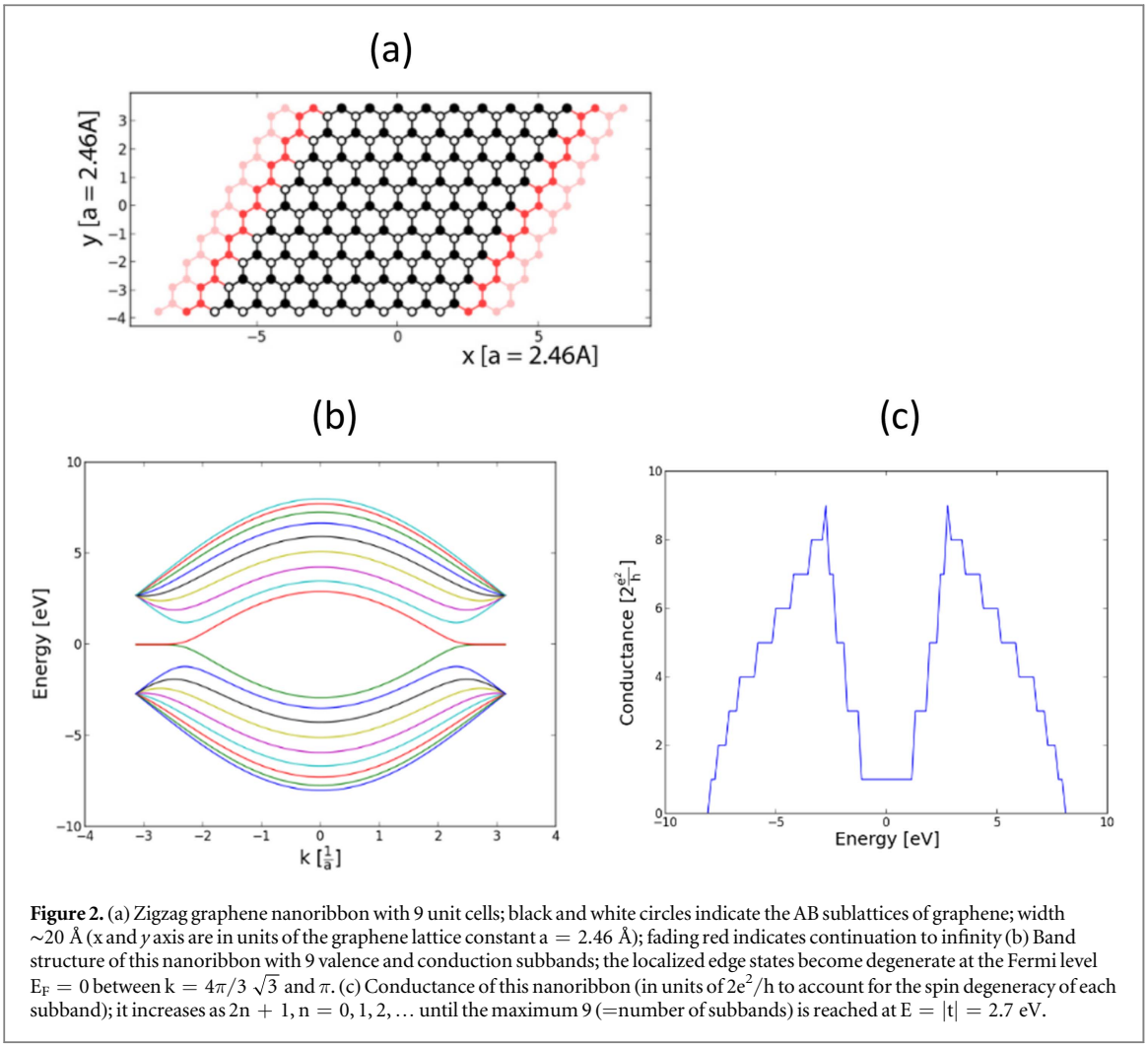

Figure 2. (a) Zigzag graphene nanoribbon with 9 unit cells; black and white circles indicate the AB sublattices of graphene; width ~20 Å (x and *y* axis are in units of the graphene lattice constant a = 2.46 Å); fading red indicates continuation to infinity (b) Band structure of this nanoribbon with 9 valence and conduction subbands; the localized edge states become degenerate at the Fermi level $E_F = 0$ between $k = 4\pi/3\sqrt{3}$ and π. (c) Conductance of this nanoribbon (in units of $2e^2/h$ to account for the spin degeneracy of each subband); it increases as $2n + 1$, $n = 0, 1, 2, \ldots$ until the maximum 9 (=number of subbands) is reached at $E = |t| = 2.7$ eV.

perpendicular magnetic field B in z-direction and leads in the x-direction [22])

$$t_{ij}(\Phi/\Phi_0) = t\exp\left[-i\Phi/\Phi_0(x_i - x_j)(y_i + y_j)/2\right] \quad (2)$$

with $\Phi_0 = h/e$ being the magnetic flux quantum. To benchmark our results, we checked our adaption of Kwant by reproducing the $2n + 1$ dependence ($n = 0, 1, 2,.$) for the dimensionless quantum conductance [7] (expressed in the unit of quantum conductance $2\,e^2/h$) and the unconventional quantum Hall effect [29] for the graphene zigzag nanoribbons used as leads to the DRN. Figure 2(a) shows the graphene nanoribbon with a width of ~8 a (a = 2.46 Å is the graphene lattice constant) used later as lead, the location at $E = 0$ of the degenerate zigzag edge state (figure 2(b)) which provides the conduction channel (figure 2(c)) in the energy region later discussed.

Metallic leads are needed for calculations of electronic transport. Zigzag nano ribbons were chosen because they are always metallic due to the edge state and therefore provide a conduction channel at the Fermi energy $E = 0$, whereas armchair ribbons are semiconducting or, depending on the width, metallic with vanishing DOS at $E = 0$ [7]. On the other hand, quantum dots with armchair edges have larger bandgaps, so overall, one would expect an electronic structure with fewer states (or no states in the case of armchair ribbons as leads) in the region of interest that contribute to the transport properties.

3. Results and discussion

3.1. Electronic properties

The electronic properties of the DRN are determined by the energy spectrum and the wavefunctions nearest to the Fermi energy. The B3LYP-DFT/6-31G results are summarized in figure 3. To analyze the spectrum of the DRN it is helpful to look into the energy level diagram of the (non-interacting) constituent parts: the outer C168 ring (gap $E_G = 1.25$ eV), the BN120 ring constituting a barrier ($E_G = 6.11$ eV), and the C96 dot ($E_G = 1.95$ eV).

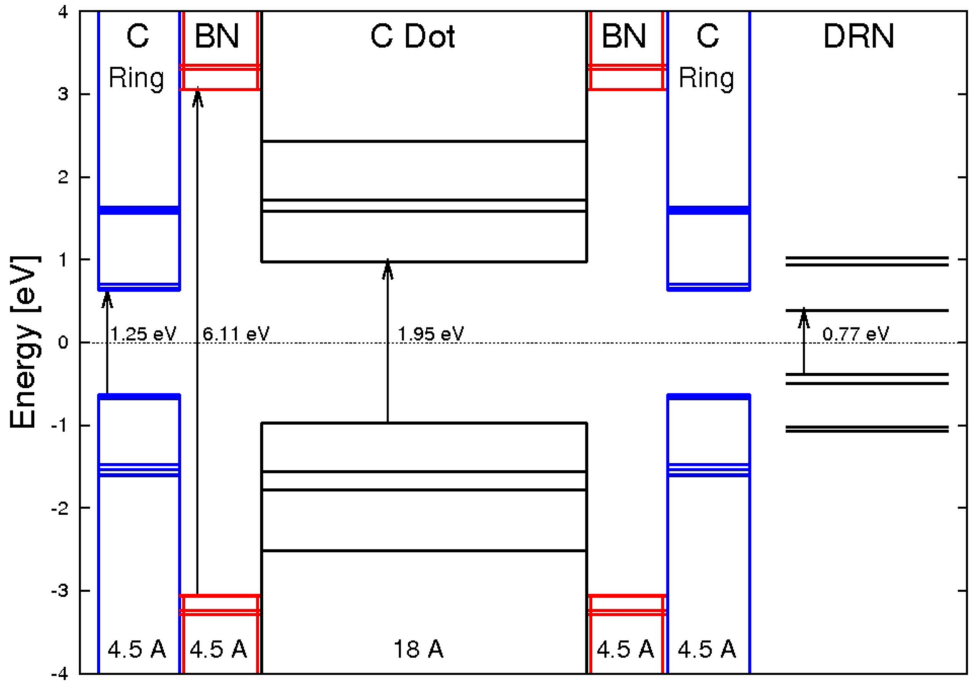

Figure 3. Molecular Orbital energy level diagram of the DRN compared to the (non-interacting) constituent parts: the outer C168 ring ($E_G = 1.25$ eV), the BN120 ring barrier ($E_G = 6.11$ eV), and the C96 dot ($E_G = 1.95$ eV). Due to symmetry, all HOMO and LUMO orbitals are doubly degenerate. The structures are aligned with the gap midpoint defined as $E_F = 0$. Only energy levels close to E_F are shown. The width of the ring, barrier, and dot corresponding to a cross section of the DRN is indicated in Å.

The positions of the energy levels of the highest occupied and lowest unoccupied MOs of these constituent parts define a single particle well structure where the potential energy bottom of the ring is $(1.95 - 1.25)/2$ eV $= 0.35$ eV below the bottom of the central dot separated by a barrier of $(6.11 - 1.25)/2$ eV $= 2.43$ eV due to the BN ring. It is therefore to be expected that the wavefunctions nearest to the Fermi energy E_F will be confined to the outer ring. This is also not surprising because the zigzag edge states of a graphene structure are always nearest to E_F.

When the interaction between these constituent parts is turned on, that is, the electronic properties of the DRN as shown in figure 1 are calculated, the gap is reduced to 0.77 eV, which is only slightly larger than the 0.65 eV gap obtained for the corresponding C384H48 graphene quantum dot. The highest occupied and lowest unoccupied MOs are shown in figure 4. As expected from the nature of the well structure, the doubly degenerate HOMO and LUMO orbitals are confined to the outer ring as is the HOMO-1 and LUMO + 1 state. The doubly degenerate HOMO-2 and the LUMO + 2 orbitals are the first wavefunctions that are mainly confined to the inner dot. Due to the twofold degeneracy of the HOMO and LUMO orbitals, each orbital alone does not reflect the symmetry with respect to $2\pi/3$ rotation about its center but a linear combination of these would. The non-degenerate HOMO-1 and LUMO + 1 clearly reflect the symmetry.

A Mulliken population analysis reveals that significant charge transfer occurs within the DRN, the main feature being a positively charged inner quantum dot and a negatively charged BN barrier: the C96 dot has a net charge of +2.6 e, the BN ring carries a charge of −6.4 e, the outer C168 ring −2.6 e, and the passivating 48 H atoms +6.4 e. A more detailed and better picture of the charge distribution within the DRN can be seen in the electrostatic potential (ESP) map given in figure 5: shades of blue indicate relative absence of electrons (around the B atoms) and red relative abundance of electrons (around N and sets of C atoms). It is to be expected that the distribution of positive and negative charges in different regions of the DRN and the confinement of different orbitals near the Fermi energy either in the outer ring or inner dot lead to novel transport properties different from those of a regular graphene quantum dot. This will be explored in the next section by calculating quantum transport properties using a tight binding model.

3.2. Quantum transport properties

In order to explore the transport properties of a dot-ring nanostructure consisting of graphene and h-BN we used the tight binding Hamiltonian described in section 2 and the software package Kwant [22]. The results are summarized in figure 6.

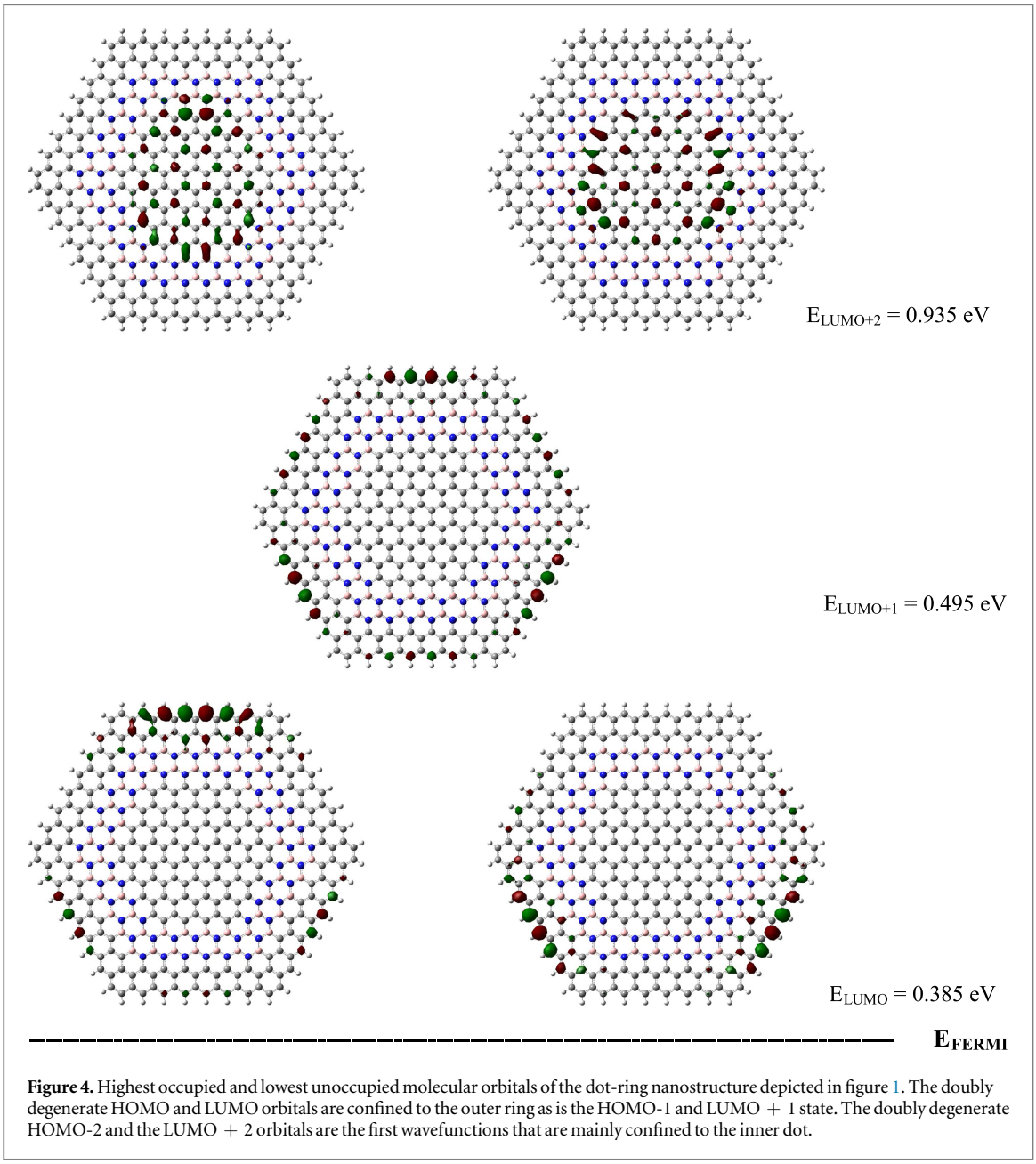

Figure 4. Highest occupied and lowest unoccupied molecular orbitals of the dot-ring nanostructure depicted in figure 1. The doubly degenerate HOMO and LUMO orbitals are confined to the outer ring as is the HOMO-1 and LUMO + 1 state. The doubly degenerate HOMO-2 and the LUMO + 2 orbitals are the first wavefunctions that are mainly confined to the inner dot.

The DRN is shown in figure 6(a). It has a diameter of ∼50 Å (20 a with a = 2.46 Å being the lattice parameter of graphene). The width of the graphene ribbon leads is ∼20 Å. A narrow BN barrier ring separates the inner dot with a diameter of ∼25 Å from the outer graphene ring. An analysis of the tight binding wavefunctions around E_F shows that they are again-as found before in the first principle study-localized in the outer ring.

The tight binding structure represents a larger, more rounded structure (∼50 Å diameter) than the *ab inito* one (hexagon diameter ∼37 Å). It also has a mix of zigzag and armchair edges. Passivating H atoms at the edge atoms are not necessary because each atom is assumed to contribute one π orbital, each atom has the same on-site parameter independent of its location. Despite the differences, an analysis of the eigenvalues and eigenvectors around the Fermi energy reveals qualitatively similar properties: the tight binding wave functions corresponding to eigenvalues immediately around E_F are again localized in the outer ring, followed by eigenvalues and wavefunctions localized in the inner dot, i.e., they show the properties desired for a dot-ring nanostructure. One can therefore expect, that the transport properties found for the tight binding structure will describe (at least qualitatively) the properties expected from a full *ab inito* transport calculation for the hexagonal structure.

To benchmark the DRN results, we first compute the conductance of the corresponding graphene dot with a diameter of 50 Å. (see figure 6(b). It shows the expected structure with resonances symmetric around $E_F = 0$. The peak maximum is defined by the conductance value of the graphene ribbon in this energy range which is at the first plateau of 2 e^2/h (see figure 2(c). The conductance of the DRN is shown in figure 6(c). It shows a slightly

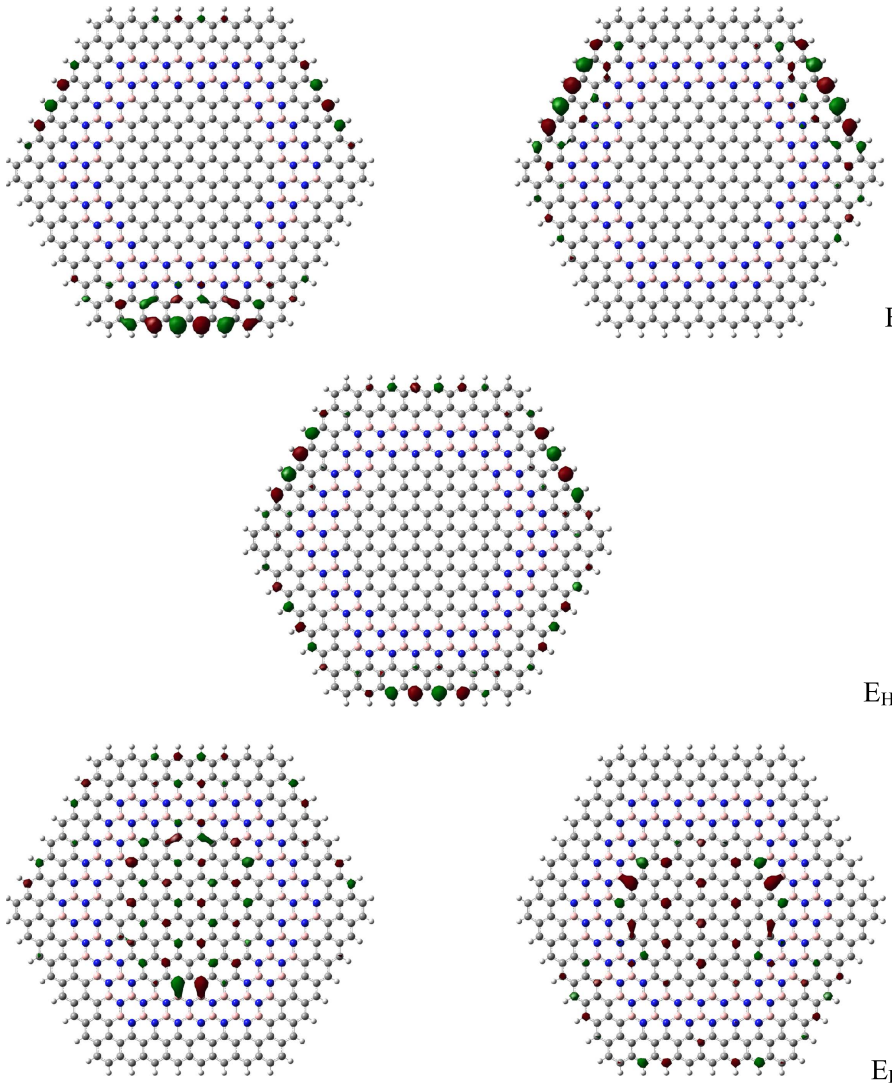

Figure 4. (Continued.)

narrower peak structure and is asymmetric around $E_F = 0$ with smaller transmission probabilities in the positive energy range.

In the tight binding model a gate voltage or a p-n junction can simply be modeled by adding to the on-site parameters u_i a potential $\pm U_G$ for p (n) regions [22, 30]. Therefore, to model a negative gate potential applied to the inner dot the on-site energy of the inner-dot C atoms is modified by $U_G = -0.5$ eV. The resulting conductance is shown in figure 6(d). The negative gate voltage increases the transmission probability in the positive energy range with a new resonance peak emerging at ~+0.3 eV. The states associated with this new resonance are two wavefunctions mainly localized on the inner dot: they are pulled down from ~0.7 eV, the corresponding eigenvalue of the DRN without applied gate voltage. A positive gate voltage of $U_G = +0.5$ eV pushes these two eigenvalues to 0.75 and 0.79 eV and the associated wavefunctions are localized on the ring, not on the inner dot.

The current can be calculated by using the Landauer formula [23, 31]

$$I = \frac{2e}{h} \int_{-\infty}^{\infty} T(E)[f_L - f_R]\, dE \tag{3}$$

T(E) is the transmission function, f_L (f_R) the Fermi–Dirac distribution for the left (right) lead. For low temperatures, the upper limit can be approximated by the Fermi energy $E_F{}^L$ ($E_F{}^R$) with f_L (f_R) = 1 in the respective integration regions so that the integral becomes $\int_0^{\Delta} T(E)\,dE$ if $E_F{}^L$ is shifted by $+\Delta$ and $-\int_{-\Delta}^{0} T(E)\,dE$ when shifted by $-\Delta$ (Δ in eV; $E_F{}^R$ kept at 0). The relation between the transmission function T(E) and conductance G(E) plotted before is

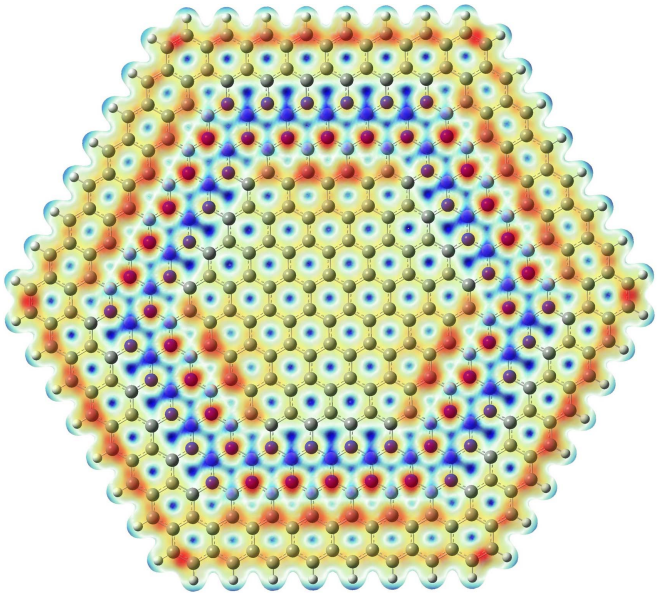

Figure 5. The electrostatic potential (ESP) map of the DRN shown in figure 1. Shades of blue (red) indicate relative absence (abundance) of electrons.

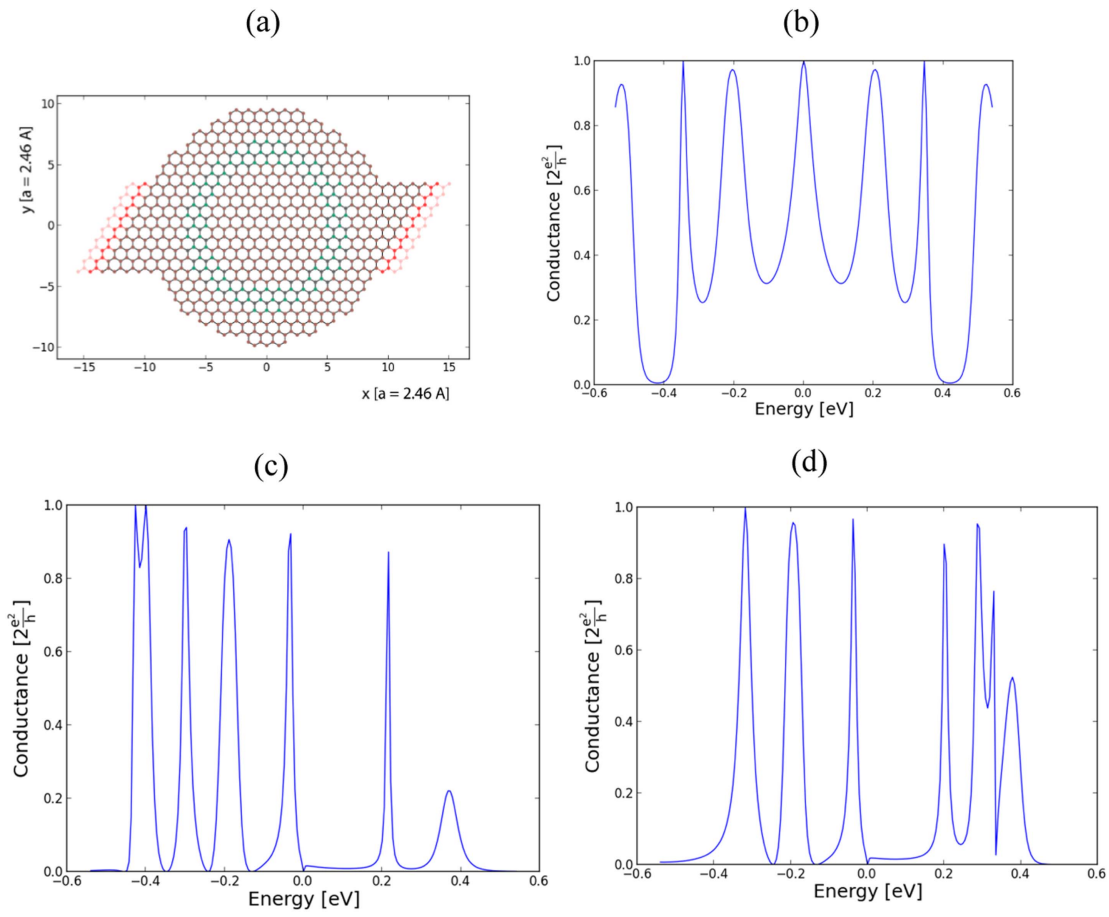

Figure 6. (a) Geometry of the DRN with an outer ring radius of 10 a (x and *y* axis are in units of the graphene lattice constant a = 2.46 Å), a second ring with radius of 7 a, and an inner dot radius of 5 a. The width of the leads is 8 a. N atoms are green, B atoms grey, C atoms brown. Fading red indicates continuation to infinity. (b) Conductance of a graphene dot with resonances symmetric around $E_F = 0$. (c) Conductance of the DRN. (d) Conductance of the DRN when the on-site energy of the C atoms of the inner dot is modified by $U_G = -0.5$ eV to model a negative gate potential applied to the inner dot.

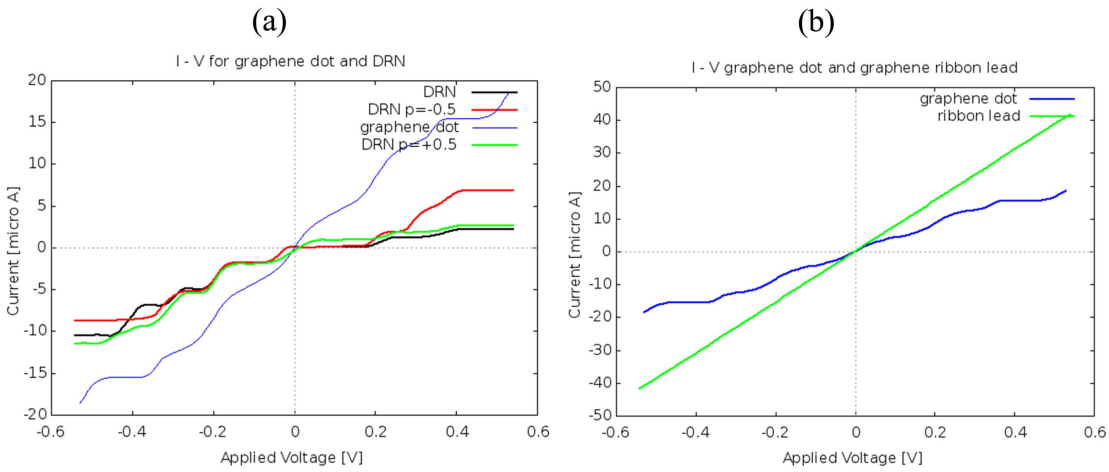

Figure 7. (a) I–V characteristics of the DRN without (black) and with an applied gate voltage (red and green) at the central dot compared to a graphene dot (blue). (b) I–V characteristics of a graphene dot (blue) compared to the graphene ribbon leads (green).

$$G(E) = 2e^2/hT(E). \quad (4)$$

With $2e^2/h = 7.75 \times 10^{-5}\,[\Omega^{-1}]$, the resulting currents are plotted in figure 7.

For the graphene dot the conductance with resonances symmetric around $E_F = 0$ (see figure 6(b)) leads to a current increase from -20 μA to $+20$ μA symmetric around 0 when the bias voltage changes from -0.6 V to $+0.6$ V (blue curve in figure 7(a)). Sections of steeper increases followed by flatter or plateau-like segments approximate a straight line with an overall slope of $\Delta I/\Delta V \sim 20$ μA/0.6 V $\sim$33 μA/V. For comparison we show the I–V characteristics of the graphene zigzag ribbon in figure 7(b): since between -0.6 eV and $+0.6$ eV its conductance has a constant value of $2e^2/h$ (see figure 2(c); the zigzag edge state provides the only conduction channel) the current increases linearly with a slope of $\Delta I/\Delta V \sim 45$ μA/0.6 V $\sim$ 75 μA/V corresponding to a resistivity of $\sim$13 kΩ. The order of magnitude is consistent with experimental results [32] that show that the resistivity of a ribbon increases as the width decreases with a resistivity between 10–15 kΩ for a ribbon width around 20 nm.

For the DRN, the plateaus in the I–V curve are more pronounced compared to the graphene dot due to the sharper peak structure in the conductance (see figure 6(c)), but the noticeable difference is the asymmetry between a negative and positive applied voltage resembling the IV characteristics of a n-p junction: between -0.6 V and zero the current changes from -10 μA to zero, then it stays zero until $\sim$0.2 V to finally reach a value of only $\sim$2 μA, 5 times smaller than that for a negative voltage and 10 times smaller than the current found for the graphene dot. When the gate potential of -0.5 eV is applied to the inner dot (red curve in figure 7(a)) the asymmetry is partially lifted: for positive voltage, the current is still zero until $\sim$0.2 V but then increases to a value of $\sim$7 μA for 0.6 V, comparable to the value of approximately $-$ 8 μA at -0.6 V. For a positive gate potential of $+0.5$ eV (green curve in figure 7(a)) the asymmetry persists and the conductance resembles the conductance of the DRN with zero gate voltage.

4. Summary and conclusion

In summary, we have analyzed the electronic and quantum conduction properties of a novel quantum dot-ring nanostructure consisting of an outer graphene ring separated from an inner graphene quantum dot by a BN ring serving as barrier. The distribution of positive and negative charges in different regions of the DRN and the confinement of orbitals near the Fermi energy either in the outer ring or inner dot obtained from first principle calculations suggests tunable conduction properties. Exploratory tight binding quantum transport calculations show that asymmetry in the conductance resonances of the DRN leads to asymmetric I–V characteristics which can be modified by applying a negative voltage potential to the central graphene dot and have dot wave functions contributing to the conductance.

Dot-ring nanostructures can be fabricated [33] by cutting a slice of a core–shell nanowire with a potential barrier between the core and the shell. The dimensions of experimentally fabricated heterostructures are certainly larger. Here, for an exploratory calculation, the dimensions of the quantum dot-ring structure were chosen to allow for reasonable computer times. For a larger ring-dot structure which might be experimentally feasible, we would still expect that the mechanism responsible for the transport properties, i.e., the shifting of the dot wave function to allow for a resonance with the ring and lead wave function, will hold.

Acknowledgments

Helpful discussions with Gaoxue Wang and Kevin Waters are gratefully acknowledged. The generous support with computer time by Michigan Tech's High Performance Computer Center is very much appreciated.

ORCID iDs

Max Seel https://orcid.org/0000-0002-1535-9900
Ravindra Pandey https://orcid.org/0000-0002-2126-1985

References

[1] Novoselov K S, Geim A K, Morozov S V, Jiang D, Zhang Y, Dubonos S V, Grigorieva I V and Firsov A A 2004 *Science* **306** 666–9
[2] Geim A K and Novoselov K S 2007 *Nature Mat.* **6** 183–91
[3] Stampfer C *et al* 2011 *Front. Phys.* **6** 271–93
[4] Sun H, Wu L, Wei W and Qu X 2013 *Materials Today* **16** 433–42
[5] Lee J *et al* 2016 *Nature Physics* **12** 1032–6
[6] Zhong X, Pandey R and Karna S P 2012 *Carbon* **50** 784
[7] Wakabayashi K, Sasaki K, Nakanishi T and Enoki T 2010 *Sci Technol Adv Mater* **11** 054504
[8] Fomin V M (ed) 2014 *Physics of Quantum Rings, Nano Science and Technology* (Berlin Heidelberg: Springer)
[9] Bahamon D A, Pereira A L C and Schulz P A 2009 *Phys. Rev.* B **79** 125414
[10] Wurm J, Wimmer M, Baranger H U and Richter K 2010 *Semicond. Sci. Technol.* **25** 034003
[11] Potasz P, Guclu A D and Hawrylak P 2010 *Phys. Rev.* B **82** 075425
[12] Potasz P, Guclu A D, Voznyy O, Folk J A and Hawrylak P 2011 *Phys. Rev.* B **83** 174441
[13] da Costa D R, Chaves A, Zarenia M, Pereira J M Jr, Farias G A and Peeters F M 2014 *Phys. Rev.* B **89** 075418
[14] Britnell L, Gorbachev R V, Geim A K, Ponomarenko L A, Mishchenko A, Greenaway M T, Fromhold T M, Novoselov K S and Eaves L 2013 *Nature Communications.* **4** 1794
[15] Loh G C and Pandey R 2015 *J. Mater. Chem.* C **3** 5918–32
[16] Zipper E, Kurpas M and Maska M M 2012 *New Journal of Physics* **14** 093029
[17] Janus-Zygmunt I, Kedzierska B, Gorczyca-Goraj A, Zipper E and Maska M M 2016 *International Journal of Modern Physics* B **30** 1642013
[18] Frisch M J *et al* 2009 *Gaussian 09, Revision D.01* (Wallingford CT: Gaussian, Inc.)
[19] Becke A D 1993 *J. Chem. Phys.* **98** 5648–52
[20] Lee C, Yang W and Parr R G 1988 *Phys Rev* B **37** 785–9
[21] Schumacher S 2011 *Phys. Rev.* B **83** 081417
[22] Groth C W, Wimmer M, Akhmerov A R and Waintal X 2014 *New J. Phys.* **16** 063065 see also: (https://kwant-project.org/)
[23] Landauer R 1957 *IBM J. Res. Dev.* **1** 223
Landauer R 1988 *IBM J. Res. Dev.* **32** 306 and references therein
[24] Büttiker M 1986 *Phys. Rev. Lett.* **57** 1761
[25] Jungthawan S, Limpijumnong S and Kuo J L 2011 *Phys. Rev.* B **84** 235424
[26] Abergel D S L 2016 *J. Phys.: Condens. Matter* **29** 075303
[27] Peierls R E 1933 *Z. Phys* **80** 763
[28] Hofstadter D R 1976 *Phys. Rev.* B **14** 2239
[29] Gusynin V P and Sharapov S G 2005 *Phys. Rev. Lett.* **95** 146801
[30] Zarenia M, Pereira J M Jr, Peeters F M and Farias G A 2013 *Phys. Rev.* B **87** 035426
[31] Curevas J C and Scheer E 2010 *Molecular Electronics : An Introduction to Theory and Experiment* (Singapore: World Scientific) (chapter 13)
[32] Chen Z, Lin Y M, Rooks M J and Avouris P 2007 *Physica.* E **40** 228-232
[33] Lauhon L J, Gudiksen M S, Wang D and Lieber C M 2002 *Nature* **420** 57–61